Performance study of Whale-Inspired Wind Turbine Blade at Low Wind Speed Using Numerical Method

Open Access

Bashir Isyaku Kunya[1,*], Clement Olaloye Folayan[2], Gyang Yakubu Pam[2], Fatai Olukayode Anafi[2], Nura Mu'az Muhammad[1]

[1] Department of Mechanical Engineering, Kano University of Science and Technology, Wudil, Nigeria
[2] Department of Mechanical Engineering, Ahmadu Bello University, Zaria, Nigeria

ARTICLE INFO	ABSTRACT
	A country like Nigeria has a vast resource of untapped renewable energy potential. It has wind speed ranging up to 13.8 m/s in Jos (the best among the most promising wind potential locations). Unfortunately, these wind speeds are considered quite low when compared to an international market which designs for turbine rated speed far higher than Nigeria's average wind speeds, and the significant variance of the average wind speeds decreases their useful potential. The efficiency of the horizontal axis wind turbine decreases when it is not operating under design conditions, which indicate the need for the technology specific to the low wind speed conditions of Nigeria. Modification of wind turbine blade leading edge is one of the best ways known for boosting the operating angle of the blade for better performance at low wind speed. This research work involved Three-dimensional flow simulation of three-bladed wind turbine rotor at low wind speed by modifying the blades' leading edges (introducing sinusoidal bumps) using the Spalart-Allmaras turbulence model and pseudo transient for solution stability. The coefficients of performance investigated for the rotating wind turbine blades with leading-edge bumps and those with the smooth leading edge. The results show that the bumpy blade can perform better than the smooth one in the low wind speed condition even at a lower angle of attack (6^0); the bumps act as passive flow control devices.

1. Introduction

Wind power potential locations in some cities in Nigeria (Minna, Sokoto, Kano and Jos) experiences average wind speeds in the range of 3.65 to 5.24 m/s [1]. According to Ahmed *et al.,* [2], the highest average wind speed in Nigeria was 10.12m/s found in Jos. A recent study by Oyewole [3] found that the highest average wind speed in Nigeria is up to 13.8m/s in Jos. However, these wind speeds are considered quite low when compared to an international market which designs for turbine rated speed far higher (in most cases above 15 m/s) than Nigeria's average wind speeds.

Furthermore, the significant variance of the average wind speeds decreases their useful potential. The efficiency of the horizontal axis wind turbine decreases when it is not operating under design conditions, which indicate the need for the technology specific to the low wind speed conditions of Nigeria. The primary approach to improving the performance of a wind turbine blade at low wind speeds is to increase its angle of attack. The recurring problem is that increasing the angle of attack eventually forces the blade to stall. If technology could be developed to boost the operating angle of the blade, the prospect exists for improvement of wind turbine performance.

Fish *et al.,* [4] found that the unique leading edge of the Humpback whales (Megaptera Novaeangliae) (Figure 1) pectoral flippers that incorporate distinct bumps or "tubercles" might play a role in their feeding process. They noted that the existence of these bumps benefits them with increased manoeuvrability relative to other baleen whales, and their evolutionary adaptation of the "bubble wall hunting" process where small radius turns are especially beneficial for their enhanced feeding success. Humpback whales were found to use their flippers at higher operating angles before stall would occur, which enable it to make very tight turns in manoeuvring to secure their food.

Fig. 1. Humpback whale [5]

Effectiveness of tubercles was evaluated by Miklosovic *et al.,* [6] by developing two CAD models of a foil simulating the planform shape and cross-section of a humpback whale pectoral flipper. One CAD model had the smooth leading edge of a conventional foil, while the other included eight sinusoidal bumps. The results showed increased peak lift, equal or reduced drag, and a delay in a stall from approximately 12° angle of attack (AoA) for the conventional foil to about 17.5° AoA for the foil with tubercles. This represents a performance improvement.

Modification of wind turbine blade leading edge by introducing tubercles (bumps) can improve its performance the same way it does for the humpback whale. Many researchers have worked on the advantage of modifying airfoil leading-edge on its performance by improving the operating angle of the airfoil. Hansen *et al.,* [7] studied the influence of bump height (from 3% to 11% of the chord) experimentally, and sinusoidal wavelength (from 11% to 86% of the chord) at the leading edge of NASA 65-021 and NASA 0021 foils. The results show that the tubercle leading edge was more beneficial for the NASA 65-021 foil than for the NASA 0021 foil and that both tubercle foils showed increased maximum lift coefficient and a larger stall angle than the conventional foil. Increasing wavelength improved stall characteristics, but also slightly reduced the maximum lift coefficient for both foils. Measurements of lift and drag were performed versus angle of attack over a range of Reynolds numbers from 1.2 x 105 to 2.74×10^5. Ahmed [8] used the standard k-ε model as the turbulence modelling technique and carried out a numerical simulation of the effect of tubercles on the flow characteristics around NASA 0012 airfoil at Reynolds number between 65,000 and 1,000,000 and the angle of attack varied from 0° to 250°. They found that tubercles delayed stall at a higher angle of attack. For both the regular and tubercle airfoils the maximum value of lift coefficient and the angle at which stall occurs increases with Reynolds number. The values of the drag coefficient of tubercle airfoil are greater than those of conventional airfoil.

Turbine blades numerical investigation was done by Carija *et al.,* [9] who studied the aerodynamic effect of waving bumps on its leading edge. A blade with NACA 0012 cross-section and sinusoidal-shaped bumped leading edge (LE) and one with the same cross-section profile but with straight leading edge were simulated. The Reynolds number of 180000 was used for a range of angle of attack from 0° to 30°. At an angle of attack larger than 10^0, the bumped blade has shown an increase in the lift (3% to 9.5%) and decreased drag, while negligible differences in the lift and a smaller drag exhibited for the angle of attack lower than 10°. The sinusoidal leading edge also delayed the stall crisis, increasing the critical angle of attack by approximately 50 over the one for the blade with a straight leading edge.

The effect of protuberances at the leading edge of a thick airfoil (S809) was investigated using computational fluid dynamics (CFD) method in 10^6 Reynolds number [10]. The results revealed that, at low angles of attack before the stall region, lift coefficient decreased slightly rather than the baseline model. However, the modified airfoil has a smooth stall trend while the baseline airfoil lift coefficient sharply reduced due to the separation which occurred on a suction side.

A numerical analysis of the flow characteristics behind the effects of leading-edge protuberances on NACA 634-021 airfoil performances was carried out at low Reynolds number [11]. It was found that the tubercle airfoil could provide more aerodynamic lift than the smooth one within the post-stall region and the stalled process was rather gentle. Within stall region, an interesting converged and diverged vortical flow in adjacent trough sections of tubercles ('bi-periodic' phenomenon) was created with the complicated evolution of the generated stream-wise counter-rotating vortex pairs, resulting in the degraded aerodynamic characteristics. For the post-stall cases, the improved airfoil performance according to them was due to the impaired flow detachment around both peak and trough sections of tubercles.

Computation of lift and drag of ONERA M6 wing have been conducted on winglet modification that reduces tip vortex. Examination of flow features at different cant angles of winglets (30°, 60° and 75°) and different angles of attack from 3° to 6° show that the wings with winglets produce higher CL/CD ratio than the normal aircraft wing without winglets up to the certain degree of angle of attack and by further increasing to a higher angle of attack its performance getting diminished [12].

Recently, Kunya *et al.,* [13] studied numerically and experimentally the effect of varying sinusoidal bumps (or tubercles) height at the leading edge of airfoil on efficiency using NASA LS (1)-0413 cross-section profiles using Spalart Allmaras turbulence model for numerical solutions. The parameters investigated include, lift, and drag, angle of attack and bumps height at very low Reynolds number of 49000. The results show that bumps on the blade leading edge have an advantage at post-stall angles of attack on the performance and varies with bumps height. Bumps height of 6% chord length was generally better in airfoil performance.

The survey of the previous studies on the effect of leading-edge airfoil tubercles (bumps) revealed that bumps allow the airfoil to operate and perform better at higher angles of attack before stall would occur (i.e. they delay stall) by providing higher maximum lift. Some investigations found that the tubercled airfoils could provide more aerodynamic lift than the smooth one within the post-stall region and the stalled process was rather gentle. It was further noticed that the leading-edge tubercles advantage on the performance of airfoil might depend on the tubercle size, type of airfoil, and Reynolds number used. Many research works were based on airfoil studies but did not include the effect of bumps [14-16]. Based on the available literature, this is the first time research on the experimental and numerical study of the effect of sinusoidal bumps at the leading edge of a rotating wind turbine blade with NASA LS (1)-0413 cross-section profile at low Reynolds Number (in the order of 10^4) was conducted. This arises the need for this research which ascertained that the innovation (of introducing blade leading bumps) is applicable.

2. Methodology

This study involves the use of computational fluid dynamic (CFD) method to find out whether wind turbine blade can perform better in the Nigerian low wind regime by mimicking the geometry of the humpback whale pectoral flippers leading edge by introducing similar bumps at the blade leading edge.

Two full span wind turbine blades (Figure 2) with varying chord length based on four metres three-bladed wind turbine rotor were developed; the straight edge leading edge blade (C-Blade) and the bumpy leading-edge blade based on BLEM-6C-40(3) S bumps size (B-Blade).

(a)   (b)

Fig. 2. Full Span Wind Turbine Blades

The blades were modelled and created the mesh in the workbench, and the simulation was carried out for the rotating blade using fluent solver. Figures 3 and 4 show the flow domain and the mesh, respectively. The Workbench session was started by checking the FLUENT CFD analysis setup option. Blade coordinate was imported into Workbench Design modeller and created blade surfaces from them. All the surfaces were filled and blended and thus created the solid volume of the blade. The blade was positioned in such a way that the leading edge is along the x-axis of the global coordinate starting from zero (0, 0, 0) at the root. It was upset along z-axis such that the blade axis is through the centre of the cylindrically shaped blade root. The fluid domain was modelled by creating two sectors with an internal angle of 120° each (Figure 3).
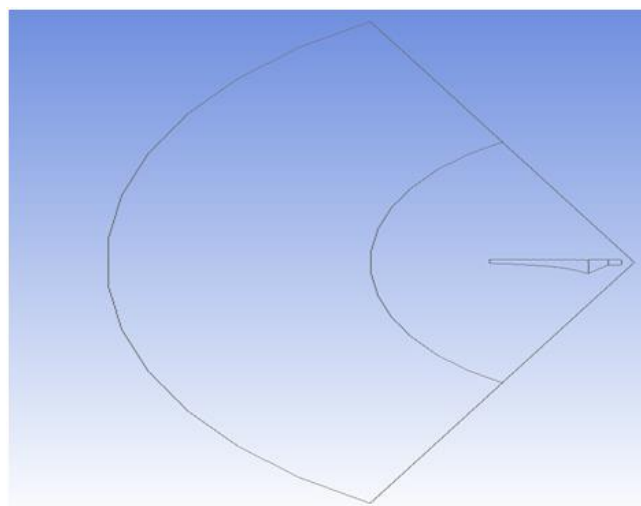
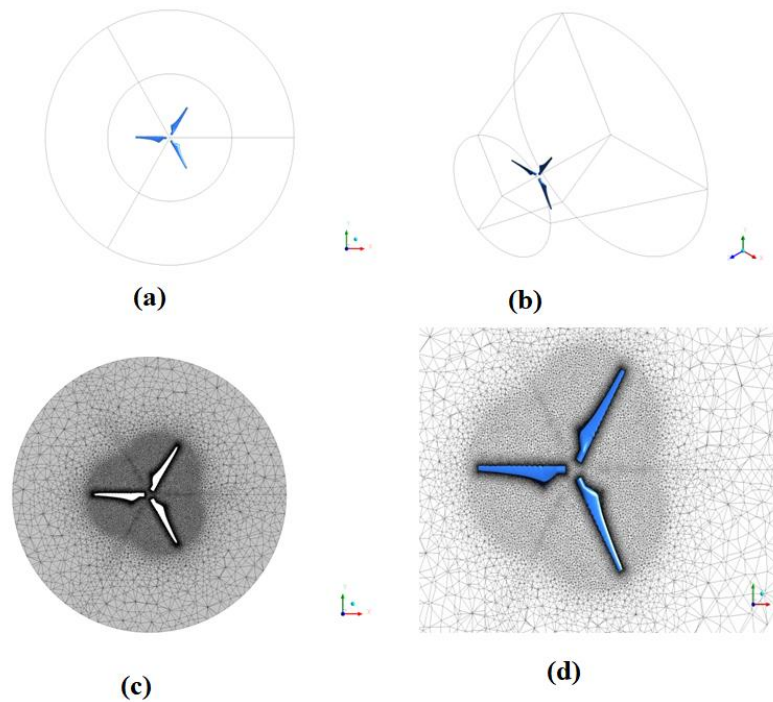**Fig. 3.** Fluid Domain Front View

The sector that represents the inlet has a radius of four-metre and positioned three-metre in front of the blade while the one that represents the outlet has a radius of eight metres and positioned six metres behind the blade. The fluid domain was created by connecting both sectors and using fill operation in the software. A subtraction operation was carried out where the blade is subtracted from the fluid domain, leaving a blade-shaped cavity in the domain; this made the geometry ready for meshing. The design modeller was closed and then opened the meshing program. Within the meshing program, a structured inflation layer (boundary layer) was added on the blade surface with

five steps. A sphere of influence was added to limit the size of the cell in the region near the blade and generated the grid. A Y$^+$ (dimensionless boundary layer parameter) value of one (1) (which is much lower than 5, the upper laminar flow limit) was used in determining the grid spacing at the boundary layer in this simulation; this help resolves the boundary layer accurately. The Y normal wall distance was calculated approximately 4.1 x 10^{-5} m or 0.000041m using a Y$^+$ value of 1 and a chord length of 0.1m at the mid-span. An unstructured grid with a hexahedral boundary layer was created in the remaining region of the fluid domain, as shown in Figure 4.

(a)   (b)
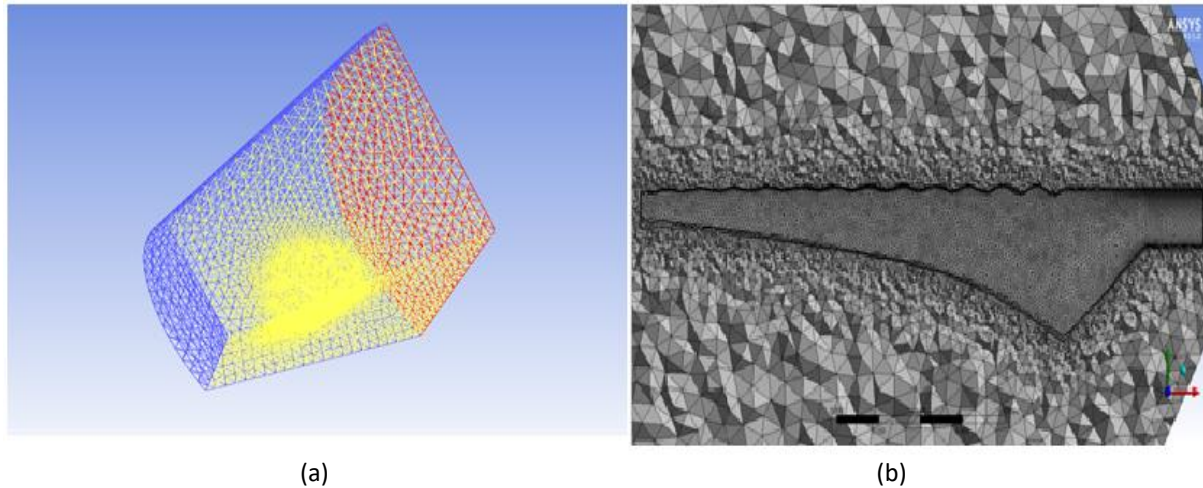
Fig. 4. Meshed domain

The inlet, outlet and periodic (Periodic because it is a rotation-based simulation) boundary conditions were specified. The meshing program was closed after and opened FLUENT. Pressure based solver was chosen in the FLUENT and assumed steady-state flow [17], similar work using this solver include [18-20]. Spalart Allmaras turbulence model was also used [21]. Under the Cell Zone Conditions, the rotation velocity of 21.3 rad/s was used after when it was determined (using equations 15 and 16, and by assuming tip speed ratio (TSR) of 6, inlet velocity of 7.1m/s, and radius of 2m). For the mesh interface settings, the periodic boundary condition type was specified as a rotational type; as a matching condition for fluid interfaces. For the solution methods, the pressure-velocity coupling scheme was used. Pseudo transient (for solution stability) and high order term relaxation is enabled for the transient formulation. The simulation is initialised from the inlet and the simulation run until convergence. One blade simulation result was extrapolated into three blades result by clicking on views from the FLUENT main menu after convergence. In the Views menu, the Define button was checked under Periodic Repeats. In the periodic repeats, the periodic type was specified as Rotational, Angle as 120^0 and Number of Repeats as 3. Then the two periodic surfaces under Associated Surfaces were chosen, clicked set, and then closed. The display in the FLUENT interface appeared to be a complete three-bladed rotor, as shown in Figure 5. The torque determined from one blade simulation was multiplied by three to calculate for three blades.

Fig. 5. Three blades in the fluid Domain: (a) Front View (b) Isometric view (c) Mesh view and (d) Enlarged mesh view

2.1 Governing Fluid Dynamic Equations

Fluid dynamics is the study of fluid motion that involves forces of action and reaction, i.e. forces which cause acceleration and forces which resist acceleration. The equations governing the fluid motion are the three fundamentals principles of mass, momentum, and energy conservation. These are [22]:

Continuity equation:

$$\frac{\partial \rho}{\partial t} + \nabla.(\rho V) = 0 \tag{1}$$

Navier-Stokes equation:

$$\rho \frac{\partial V}{\partial t} + V.\nabla(\rho V) = \nabla.\tau_{ij} - \nabla P + \rho F \tag{2}$$

Energy equation:

$$\rho \frac{De}{Dt} + P(\nabla.V) = \frac{\partial Q}{\partial t} - \nabla.q + \Phi \tag{3}$$

Where ∇ *is* $\left(\frac{\partial}{\partial x} + \frac{\partial}{\partial y} + \frac{\partial}{\partial z}\right)$

Presence of each term and their combination determines the appropriate solution algorithm and the numerical procedure. One or more terms might be neglected depending on the nature of physics governing the fluid motion.

2.2 Grid Independent Study

The goal of a grid dependency study is to find an independent grid solution. When conducting a new study, it is not likely that the first grid generated contains the necessary resolution to sufficiently capture the flow physics. For this work, the grid study was carried out by generating an initial grid of low resolution and then using the same meshing scheme to create grids of higher resolutions. All simulations for the grid study were conducted using the conventional blade (C-Blade) at a wind velocity of 7.1m/s; an angle of attack of 5^0 for stationary blade, and a blade pitch angle (β) of 6^0 and tip speed ratio (λ) of six and two-meter radius (for rotating blade). The results are tabulated (Table 1).

Table 1
Grid convergence study

Grid	Resolution (Cells)	Lift Coefficient	Drag Coefficient	Torque (Nm)
1	328700	0.486548	0.097121	29.054
2	527400	0.511537	0.105277	30.151
3	827500	0.527224	0.107111	30.874
4	1273000	0.529326	0.107919	30.891

As seen in Table 1, the lift coefficient changes from the first grid to the third, but insignificantly changed after the third grid, and it maintained a lift coefficient of around 0.52 from the fourth grid. Similarly, the drag coefficient varies from grid 1 to grid 3 but kept a close value after grid 3 with an approximate drag coefficient of 0.107. The torque value was maintained at approximately 30.8 Nm. Due to this, the third grid with a resolution of 827500 cells, was chosen as the bases for all the grids in this work.

2.3 Boundary Conditions

The governing fluid dynamic equations were solved to obtain the pressure and velocity fields within the flow domain to calculate for lift and drag forces, boundary conditions were specified. The inlet and outlet fluid velocities were defined as the free airstream velocity (V_0).

2.4 Aerodynamic Forces

A fluid flowing past an airfoil causes the fluid to divert from its original path, such change in direction lead to changes in the pressure and the velocity of the fluid. The fluid experiences resistance forces (frictional forces) as it flows due to its viscosity. This force and the force arising from the pressure over the surface of the body are collectively the resultant force exerted by the fluid on the body, known as the aerodynamic force. The aerodynamic force resolved customarily into two orthogonal components that are directionally referred to the free stream velocity (*V*) [23]:
  i.   Drag-component (*D*) parallel to the direction of the relative motion
  ii.   Lift- component (*L*) perpendicular to the direction of the relative motion
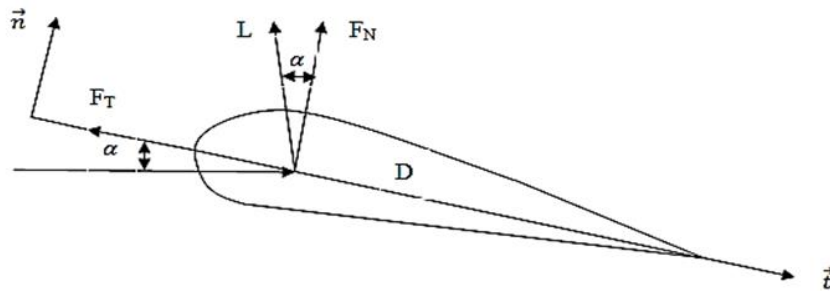   Figure 6 shows the direction of these forces exerted by the fluid on the airfoil.

Fig. 6. Airfoil Aerodynamic forces

Where D is drag force per unit length, L is lift force per unit length, F_N is total normal force per unit length, F_T is total tangential force per unit length, $\vec{t}$ is unit vector aligned to the chord, and $\vec{n}$ is unit vector perpendicular to the chord.

Pressure coefficient along airfoil (or blade) surface is given as [23]:

$$C_P(s) = \frac{P(s) - P_{static}}{P_{dynamic}} \tag{4}$$

Where, $P(s)$ is pressure along the airfoil surface, P_{static} is static pressure i.e. $P(U_o)$, $P_{dynamic}$ is dynamic pressure i.e. $\frac{1}{2} \rho U_o^2$, U_o is free stream velocity, and ρ is air density

Normal and tangential forces coefficients, respectively given as [23]:

$$C_N = \frac{F_N}{1/2 \, \rho \, U_o^2 \, C} = \frac{1}{C} \oint C_P(s) \, \vec{n} \, \overrightarrow{ds} \tag{5}$$

$$C_T = \frac{F_T}{1/2 \, \rho \, U_o^2 \, C} = \frac{1}{C} \oint C_P(s) \, \vec{t} \, \overrightarrow{ds} \tag{6}$$

Where c is airfoil chord length and $\overrightarrow{ds}$ is running along the airfoil section

Therefore the normal (F_N) and the tangential (F_T) forces are [23]:

$$F_N = \frac{1}{2} \, C_N \, \rho \, U_o^2 \, c \tag{7}$$

$$F_T = \frac{1}{2} \, C_T \, \rho \, U_o^2 \, c \tag{8}$$

Now lift (L) and drag (D) forces are [14]:

$$L = F_N \cos(\alpha) + F_T \sin(\alpha) \tag{9}$$

$$D = F_N \sin(\alpha) - F_T \cos(\alpha) \tag{10}$$

Also, lift and drag coefficients are respectively given as [23]:

$$C_L = \frac{L}{1/2 \, \rho \, U_o^2 \, C} \tag{11}$$

$$C_D = \frac{L}{1/2 \, \rho \, U_o^2 \, C} \tag{12}$$

2.5 Relationships Used for Blade Model Design and Results Analysis

i. Optimum chord length (C_{opt}) across the whole length of the blade [24]:

$$C_{opt} = \frac{2\pi r}{B} \frac{8}{9C_L} \frac{V}{\lambda V_r}$$ (13)

Where B is the blade count, λ is local tip speed ratio, V_r is local resultant air velocity (m/s), r is local radius, C_L is lift coefficient, and V is design wind speed.

ii. Blade pitch angle (β) at a particular radial station (r) [24]:

$$\beta(r) = tan^{-1}\left(\frac{2R}{3r\lambda}\right) - \alpha$$ (14)

Where R is swept radius, λ is tip speed ratio, and α is the design lift coefficient

iii. Tip speed ratio, λ [24]:

$$\lambda = \frac{V_t}{V}$$ (15)

Where V_t is the blade tip speed, and V is the wind speed.

iv. Angular velocity (ω):

$$\omega = \frac{V}{r}$$ (16)

Where V is angular velocity and r is the radius

v. Power (P):

$$P = T\omega$$ (17)

Where T is torque and ω is the angular velocity

vi. Power coefficient, C_P [25]:

$$C_p = \frac{P}{\frac{1}{2}\rho AV^3}$$ (18)

Where A is swept area, V is wind velocity, ρ is air density, and P is power.

2.6 Data Validation

The performance coefficients of the rotating C-Blades and that of B-Blades are 0.237 and 0.303 respectively. However their average value (0.27) is not up to the Betz limit (0.593) which is the maximum theoretical value, this is because according to Spalart *et al.,* [21], the Betz limit value reduces by factor of 0.5 to 0.7 in practice due to spillage loses, tip loses, e.t.c. Moreover, again in this

research work, the blades were not twisted; it is part of this research challenge that bumpy blades could not be twisted. Figure 7 shows three different blades design (OPT - tapered and twisted, UOT - twisted but not tapered, and UUT – not tapered not twisted) from the research work of Fei *et al.,* [26] who analysed the effect of blade twist and taper on blade performance. The coefficient of UOT (0.428) is the same as that of OPT even though UOT has no taper; their only difference is that UOT has lower tip speed ratio (4.32) than OPT (0.92). Because that UUT has no twist, its performance coefficient (0.210) is lower than that of other blades by about 50% and has a lower tip speed ratio (3.86). Consequently, had it been that the blade models of this current research were twisted their average coefficients of performance could reach by some factor above that of OPT and UOT values (0.428) considering that it is currently greater than that of UUT (the untwisted blade).
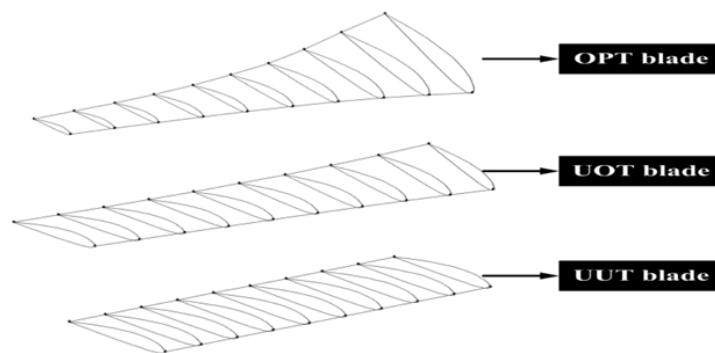

Fig. 7. Blade Twist and Taper

3. Results

This section presents the numerical results and analysis on comparing two full span wind turbine blades with varying chord length; the straight edge leading edge blade (C-Blade) and the bumpy leading-edge blade (B-Blade) based on BLEM-6C-40(3) S bumps size [10].

The analysis of the effect of leading-edge bumps with regards to the variation of lift and drag coefficients with angle of attack using the stationary C-Blade and B-Blade was done and shown in Figures 8 to 9.

Figure 8 shows that for C-Blade stall started at a 10^0 angle of attack. The B-Blade has a gentle stall regime; its lift curve did not drop as much as that of the conventional blade after the 10^0 but stayed fairly levelled. The lift curve for the C-Blade achieved a higher maximum lift coefficient (0.7) than the bumpy one (0.64) but quickly dropped below that of the bumpy blade at higher angles of attack due to stall effects (the lift coefficients for B-Blade is 0.67 which is above that of C-Blade, 0.64).

In Figure 9, drag starts at around the same point at 0^0 for both blade models. From 0^0 there is a gradual divergence of the drag values for the two blades up to a 5^0 angle of attack then converges until around 15^0. At 5^0, flow separation starts for all blades regardless of velocity involved due to profile drag becoming dominant. After the angle of 15^0 both graphs follow almost a linear path up to 25^0.
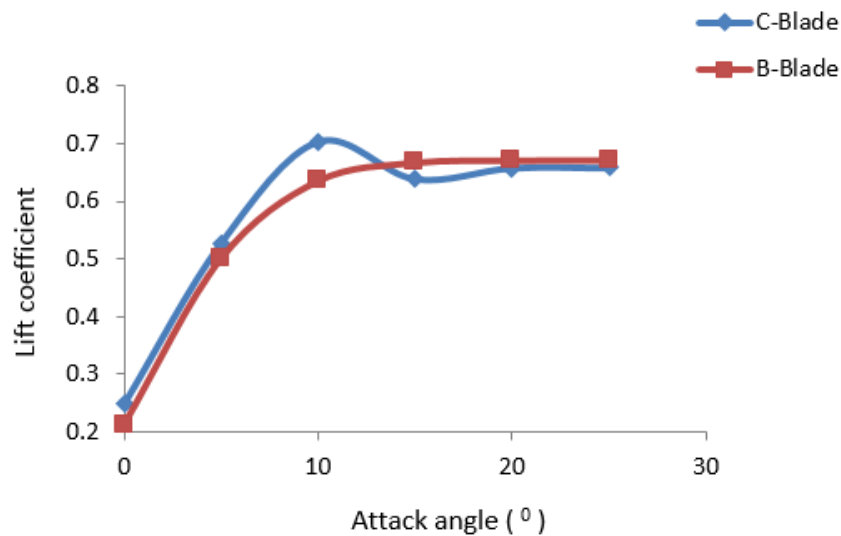
Fig. 8. Variation of lift coefficient with angle of attack at 7.1m/s
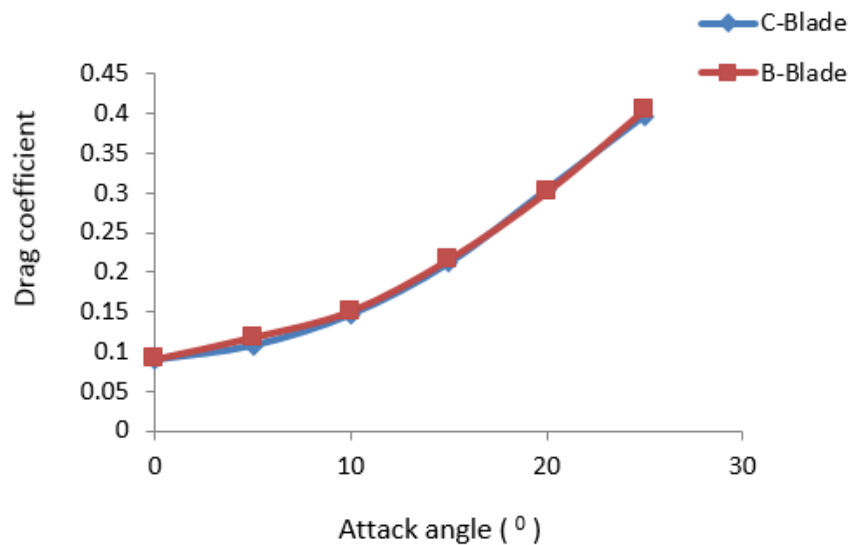
Fig. 9. Variation of drag coefficient with angle of attack at 7.1m/s

Figure 10 illustrates the Pressure contours for the conventional (C-Blade) and bumpy (B-Blade) blades mid-sections at 7.1m/s and an angle of attack of 5^0. The high-pressure region exists below the model for positive angles of attack, and the low-pressure region is on top of it (the reverse is the case for negative angles). The flow from the bottom surface to the top surface at the trailing edge creates a low-pressure region due to the pressure, and the pressure at the bottom surface is much greater than the pressure on the top surface, which creates a favourable pressure gradient in the front part but an adverse pressure gradient in the rear section. This adverse pressure gradient slows down the velocities inside the boundary layer, which causes the recirculation region close to the top surface of the airfoil. This recirculation region continues to grow upstream as more air is accelerated from bottom to top surface of the airfoil.

Figures 11 and 12 show Velocity contours for the C-Blade and B-Blade mid-sections at 7.1m/s. At an angle of attack of 5^0 (Figure 11), flow separation starts a little bit for all the blades, and the effects of profile drag become dominant.
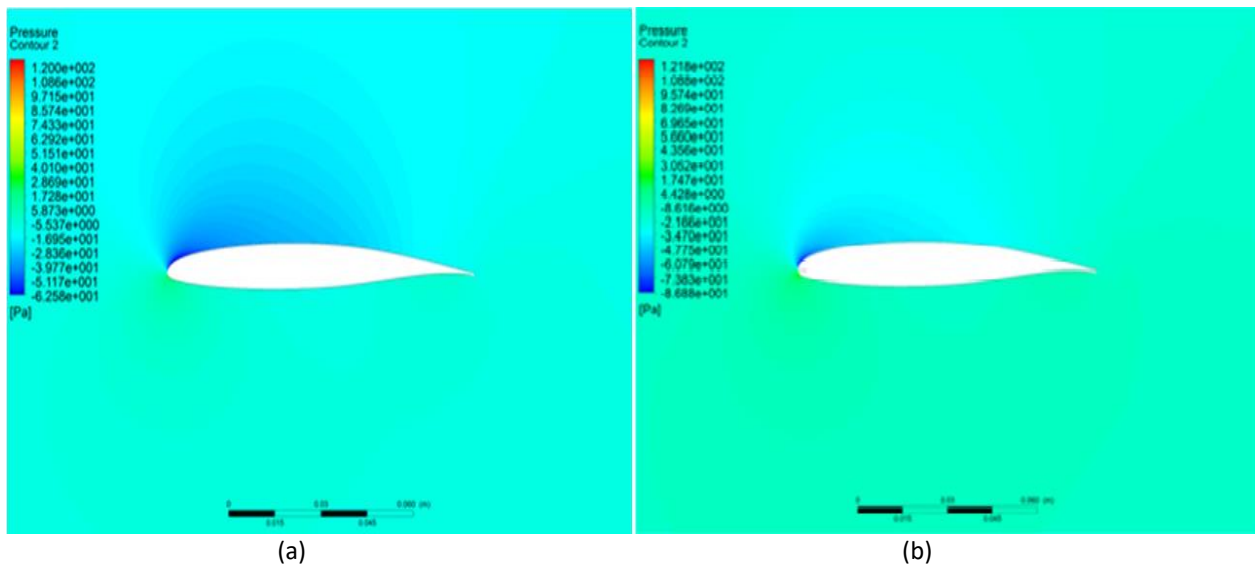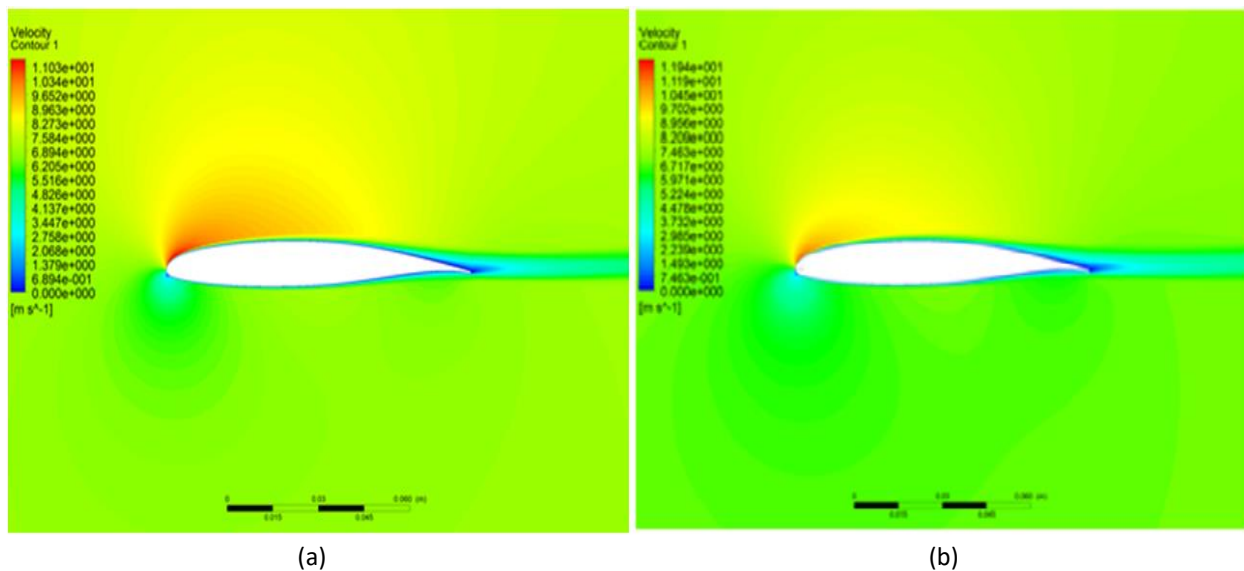
Fig. 10. Pressure contour

Fig. 11. Velocity contour at a lower angle of attack: (a) C-Blade & (b) B-Blade

The contours of velocity for the blades at a 15^0 (higher) angle of attack were compared, as shown in Figure 12. Flow separation is delayed for the B-Blade. The study revealed that bumps along the leading edge produced stream-wise vortices. These vortices carried higher momentum flow in the boundary layer, which kept the flow attached to the surface of the airfoil and, in turn, delayed separation, and thus enables a higher lift coefficient during post-stall.

The velocity vectors for the rotating blade viewed show that velocity at the blade's tip is higher and reduces toward the root, as shown in Figure 13.

The blades were simulated while rotating at 7.1m/s wind speed (V) and optimum blade pitch angle (β) of 6^0. The results (torque output) were obtained based on four (4) meter three-bladed rotor, and tip speed ratio (λ) of 6. The results (that is, torque) are thus presented as follow:

For C-Blade, $T_C = 30.87Nm$

For B-Blade, $T_C = 39.26Nm$

The output of the simulation is the torque on the blade about the axis of rotation. Therefore, the power (performance) coefficient need to be determined.

Blade tip speed, $V_t = \lambda V = 6 \; X \; 7.1 = 42.6 \; m/s$

Angular velocity, $\omega = \dfrac{V_t}{R} = \dfrac{42.6}{2} = 21.3 \; rad/sec$

Power, $P = T\omega$

Power coefficient, $C_P = \dfrac{P}{1/2\rho A V^3} = \dfrac{T\omega}{1/2\rho A V^3}$

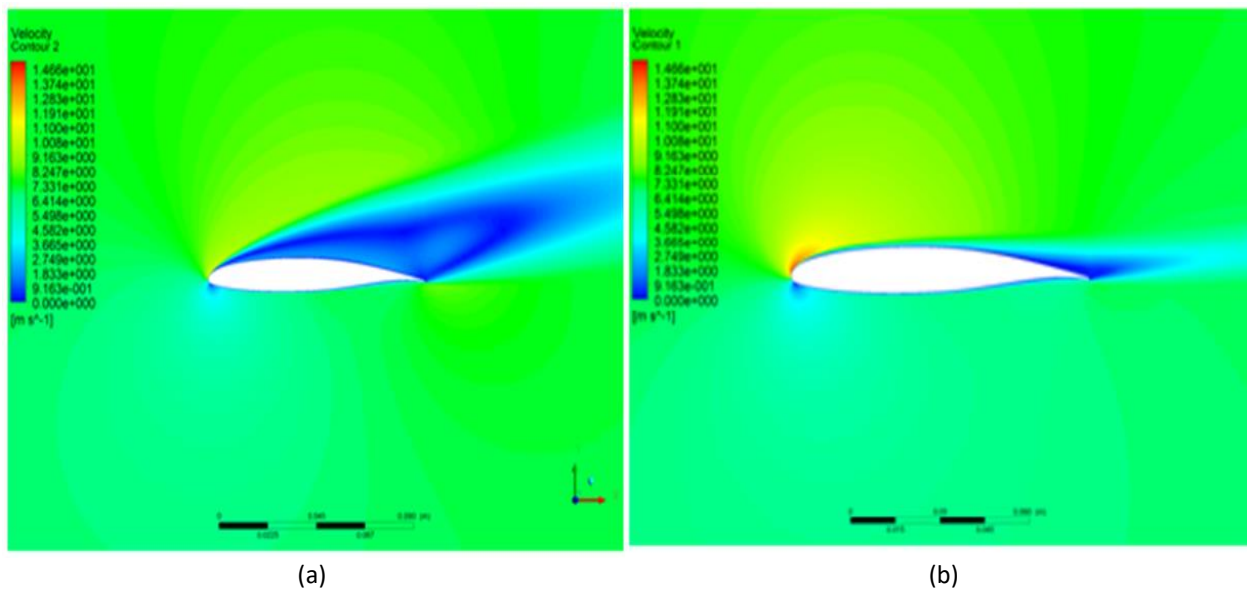
(a)   (b)

Fig. 12. Velocity contour at a higher angle of attack: (a) C-Blade & (b) B-Blade
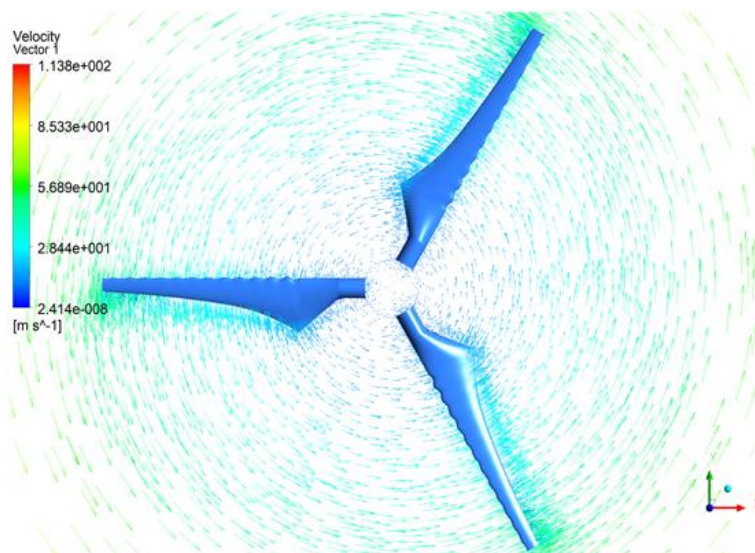

Fig. 13. Velocity vectors of the rotating blades

Comparing the power coefficients for the two blades (Table 2), the B-Blade has a higher coefficient of performance (0.303) than that of C-Blade (0.237), this shows that bumps at blade leading have more advantage on improving performance when the blade rotates at the optimal pitch

angle. The physics behind this might be because rotation accelerates the wind flow many times faster than the free stream velocity. So, the vortices generated by the bumps will carry higher momentum that can enable them to keep the flow stream more attached around the blades. The most important thing is that, when blade rotates, there is what is called spanwise loses and this reduces performance, but the introduction of bumps at the blade leading edge may reduce these losses (passive control) and strength of tip vortex and thus contribute to more lift and therefore improve performance.

Table 2
Power coefficient values for the two models

Blade type	Power coefficient
C-Blade	0.237
B-Blade	0.303

4. Conclusions

Airfoils models simulation cases from some of the previous studies and the stationary blade analysis of this research show that bumps at the leading edge have advantage only at higher angles of attack (post stall), but fortunately the simulation on the rotating blades revealed that even at lower angle of attack (6^0), bumpy blade could perform better in the low wind speed condition.

The performance coefficients of the conventional rotating blade (C-Blade) and that of the bumpy blade (B-Blade) are 0.237 and 0.303, respectively, and it shows that the introduction of the sinusoidal bumps at the leading edge of the blade has improved its performance by 27.8%. It can conclusively affirm that the whale-inspired wind turbine blade can perform very well in the low wind regime as in Nigerian wind power potential areas.

References
[1] Pam, G. Y. "Potential of Wind Energy Utilisation in Northern States of Nigeria." PhD diss., Ph. D Dissertation, Ahmadu Bello University, Zaria, Nigeria, 2008.
[2] Ahmed, Abdullahi, A. Ademola Bello, and D. Habou. "An evaluation of wind energy potential in the northern and southern regions of Nigeria on the basis of Weibull and Rayleigh models." *American Journal of Energy Engineering* 1, no. 3 (2013): 37-42.
[3] Oyewole, J. A., and T. O. Aro. "Wind speed pattern in Nigeria (a case study of some coastal and inland areas)." *Journal of Applied Sciences and Environmental Management* 22, no. 1 (2018): 119-123.
[4] Fish, Franke E., and Juliann M. Battle. "Hydrodynamic design of the humpback whale flipper." *Journal of Morphology* 225, no. 1 (1995): 51-60.
[5] Clapham, Phillip J. "Humpback whale: Megaptera novaeangliae." In *Encyclopedia of marine mammals*, pp. 489-492. Academic Press, 2018.
[6] Miklosovic, D. S., M. M. Murray, L. E. Howle, and F. E. Fish. "Leading-edge tubercles delay stall on humpback whale (Megaptera novaeangliae) flippers." *Physics of fluids* 16, no. 5 (2004): L39-L42.
[7] Hansen, Kristy L., Richard M. Kelso, and Bassam B. Dally. "Performance variations of leading-edge tubercles for distinct airfoil profiles." *AIAA journal* 49, no. 1 (2011): 185-194.
[8] Gawad, Ahmed Farouk Abdel. "Numerical Simulation Of The Effect Of Leading-Edge Tubercles On The Flow Characteristics Around An Airfoil." In *International Mechnaical Engineering Congresss & Exposition*. 2012.
[9] Čarija, Zoran, Emil Marušić, Zdenko Novak, and Sanjin Fućak. "Numerical analysis of aerodynamic characteristics of a bumped leading edge turbine blade." *Engineering Review* 34, no. 2 (2014): 93-101.
[10] Asli, Majid, Behnam Mashhadi Gholamali, and Abolghasem Mesgarpour Tousi. "Numerical analysis of wind turbine airfoil aerodynamic performance with leading edge bump." *Mathematical Problems in Engineering* 2015 (2015).

[11] Zhao, Ming, Mingming Zhang, and Jianzhong Xu. "Numerical simulation of flow characteristics behind the aerodynamic performances on an airfoil with leading edge protuberances." *Engineering Applications of Computational Fluid Mechanics* 11, no. 1 (2017): 193-209.

[12] Munshi, Adnan, Erwin Sulaeman, Norfazzila Omar, and Mohammad Yeakub Ali. "CFD Analysis on the Effect of Winglet Cant Angle on Aerodynamics of ONERA M6 Wing." *Journal of Advanced Research in Fluid Mechanics and Thermal Sciences* 45, no.1 (2018): 44-54.

[13] Kunya, Bashir Isyaku, Clement O. Folayan, Gyang Yakubu Pam, Fatai Olukayode Anafi, and Nura Muaz Muhammad. "Experimental and Numerical Study of the Effect of Varying Sinusoidal Bumps Height at the Leading Edge of the NASA LS (1)-0413 Airfoil at Low Reynolds Number." *CFD Letters* 11, no.3 (2019): 129-144.

[14] Ali, Jaffar Syed Mohamed, and M. Mubin Saleh. "Experimental and Numerical Study on the Aerodynamics and Stability Characteristics of a Canard Aircraft." *Journal of Advanced Research in Fluid Mechanics and Thermal Sciences* 53, no.2 (2019): 165-174.

[15] Hakim, Muhammad Syahmi Abdul, Mastura Ab Wahid, Norazila Othman, Shabudin Mat, Md Shuhaimi Mansor, Nizam Dahalan, and Wan Khairuddin Wan Ali. "The Effects of Reynolds Number on Flow Separation of Naca Aerofoil." *Journal of Advanced Research in Fluid Mechanics and Thermal Sciences* 47, no.1 (2018): 56-68.

[16] Tajuddin, Nurulhuda, Shabudin Mat, Mazuriah Said, and Shumaimi Mansor. "Flow characteristic of blunt-edged delta wing at high angle of attack." *Journal of Advanced Research in Fluid Mechanics and Thermal Sciences* 39, no. 1 (2017): 17-25.

[17] Guide, ANSYS Fluent User'S. "ANSYS Inc. Southpointe 275 Technology Drive Canonsburg, PA 15317." (2013).

[18] Jamil, M. M., M. I. Adamu, T. R. Ibrahim, and G. A. Hashim. "Numerical study of separation length of flow through rectangular channel with baffle plates." *Journal of Advanced Research Design* 7 (2015): 19-33.

[19] Mohamed, Abdel-Aziz Farouk Abdel-Aziz. "Hybrid Nanocrystal Photovoltaic/Wind Turbine Power Generation System in Buildings." *J. Adv. Res. Mater. Sci* 40 (2018): 8-19.

[20] Zainal, S., C. Tan, C. J. Sian, and T. J. Siang. "ANSYS simulation for Ag/HEG hybrid nanofluid in turbulent circular pipe." *Journal of Advanced Research in Applied Mechanics* 23 (2016): 20-35.

[21] Spalart, Philippe, and Steven Allmaras. "A one-equation turbulence model for aerodynamic flows." In *30th aerospace sciences meeting and exhibit*, p. 439. 1992.

[22] J. M. N. Ashgriz, "An introduction to computational fluid dynamics," in *Fluid Flow Handbook*, J. Saleh, Ed. University of Toronto. Canada: McGraw-Hill Professional 2002, pp. 24.1-24.52.

[23] J. Douglas, J. Gasiorek, J. Swaffield, and L. JACK, *Fluid Mechanics*. Pearson Prentice Hall, 2005.

[24] Schubel, Peter J., and Richard J. Crossley. "Wind turbine blade design." *Energies* 5, no. 9 (2012): 3425-3449.

[25] Rao, S., and B. B. Parulekar. "Energy Technology." *Khanna publishers* (2005).

[26] Hsiao, Fei-Bin, Chi-Jeng Bai, and Wen-Tong Chong. "The performance test of three different horizontal axis wind turbine (HAWT) blade shapes using experimental and numerical methods." *Energies* 6, no. 6 (2013): 2784-2803.